Materials and Design 183 (2019) 108087

Contents lists available at ScienceDirect

Materials and Design

journal homepage: www.elsevier.com/locate/matdes

Selective laser sintering responses of keratin-based bio-polymer composites

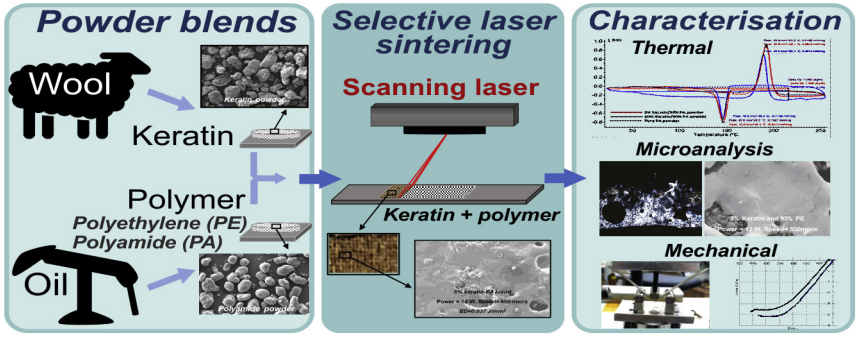
Sarat Singamneni [a, *], Rajkumar Velu [d], Malaya Prasad Behera [a], Sonya Scott [b], Peter Brorens [b], Duane Harland [b], Juliet Gerrard [c, e]

[a] Auckland University of Technology, Auckland, New Zealand
[b] Agresearch Ltd, Lincoln, New Zealand
[c] School of Biological Sciences, University of Auckland, Auckland, New Zealand
[d] Singapore University of Technology and Design, Singapore
[e] School of Chemical Sciences, University of Auckland, Auckland, New Zealand

HIGHLIGHTS

- Specific keratin-polymer blends were proved to be suitable for processing by selective laser melting.
- The presence of keratin alters the thermal responses of the base polymers.
- Keratin leads to varying degrees of slackness in the inter-particle bonding within the base polymer matrix.
- The polymer-keratin interface appears to be good.

GRAPHICAL ABSTRACT



ARTICLE INFO

Article history:
Received 14 May 2019
Received in revised form
29 July 2019
Accepted 29 July 2019
Available online 30 July 2019

Keywords:
Keratin
Polyamide
Polyethylene
Selective laser sintering
Polymer-keratin composites

Data availability statement:
The raw/processed data required to reproduce these findings cannot be shared at this time as the data also forms part of an ongoing study. Some additional data is available as Supplementary data.

ABSTRACT

Keratin-based materials have unique biological and mechanical attributes due to the protein's molecular structure and organisation. The current study evaluates the possible consolidation of keratin powders by selective laser sintering (SLS), a key enabler of additive manufacturing. The laser energy input became too intense for the thermally sensitive keratin powders. However, polymer keratin composites developed by blending with polyamide and polyethylene powders were evaluated and shown to be suitable for processing by SLS. Blends were thermally characterised to establish the initial process conditions. Morphological evaluation of the initial sintered samples allowed optimisation of the energy densities. Mechanical responses of the samples produced under these conditions were evaluated. Polymer-keratin composites were established as candidate materials for SLS. Critical attributes of these material combinations require further optimisation before these materials would be competitive in the market place.
© 2019 The Authors. Published by Elsevier Ltd. This is an open access article under the CC BY-NC-ND license (http://creativecommons.org/licenses/by-nc-nd/4.0/).

* Corresponding author.
E-mail address: sarat.singamneni@aut.ac.nz (S. Singamneni).

https://doi.org/10.1016/j.matdes.2019.108087
0264-1275/© 2019 The Authors. Published by Elsevier Ltd. This is an open access article under the CC BY-NC-ND license (http://creativecommons.org/licenses/by-nc-nd/4.0/).

1. Introduction

Selective laser sintering (SLS) and melting (SLM) are common additive processing methods for synthetic biopolymers [1]. The approaches have developed around thermoplastic materials, primarily polyethylene (PE), poly (L-lactic acid) (PLA), polymethylmethacrylate (PMMA) and polyamide (PA) because of their biomechanical and medical uses [2–6]. The processes rely on direct energy input to fuse powder particles and scanning to impose a selective pattern of fusion across a powder surface. Repetition of the process over fresh layers of powder that are thinly drawn across previously scanned layers create the three-dimensional structure. The approach uses a CO_2 laser [7] and a powder bed maintained at an elevated temperature [8] optimised for intra- and inter-layer coalescence.

SLS and SLM technologies were designed around thermoplastic materials that have high melting point temperatures. Most readily available materials derived from carbohydrates (*e.g.*, chitosan and alginate) and proteins (*e.g.*, gelatine) are not thermoplastic, and are typically damaged or destroyed at the elevated thermal temperatures used in the plastics industry [9–11]. Collagen, albumin, fibroin, elastin and keratin are different forms of protein derived from natural materials [12] with potential for use in composites. Protein-based biomaterials have recognised value as synthetic extracellular matrices, facilitating cell-cell and cell-matrix interactions and preservation of macromolecular biochemical, mechanical and structural functions [13,14]. The diverse physical and chemical properties of proteinaceous macromolecules are attractive in applications such as medical devices and bioactive surfaces. [15]. Here we focus on hard-keratins; also known as hair or tricho-keratins [16,17]. These are the basis of naturally robust materials such as hair, horn and hoof, and have intrinsic biocompatibility, biodegradability, mechanical durability and are good candidates for application as bio-based materials [17,18]. Advances in the extraction, purification and characterisation of keratins from wool, human hair and hooves [19,20] has led to uses which leverage on the specific biological properties of keratin, such as biocompatible human hair keratin derived tissue scaffolds [21] and horn and hoof keratins in non-toxic firefighting compositions [22]. Other applications range from tissue engineering [23–25] to drug delivery systems, electrodes, packaging to waste management, and bio-fertilisers [26–34].

Keratin powder quickly chars in direct laser sintering conditions. Our aim here was to evaluate the possible application of hard-keratins into SLS through blending small fractions of keratin with bio-compatible base polymers polyamide and polyethylene [35]. Blending can be a way to protect some bio-functional properties or enhance bio-conductivity and mechanical properties [36]. There is no *a priori* data available for this approach with keratin. We used differential scanning calorimetry (DSC) as a primary means of establishing a viable process. Based on the working ranges of the energy densities, single layer sintered samples were produced for more detailed morphological and mechanical analysis.

Although blending with keratin appears not to have been investigated with additive manufacturing, there has been some promising research in related fields. These include approaches which use combined high pressure and shear deformation to blend solid components [37]. Jiang et al. fabricated poly(hydroxybutylate-cohydroxyvalerate) (PHBV) and modified keratin dissolved in hexafluoroisopropanol (HFIP) to create nanofibrous mats using electrospinning [38]. Zoccola et al. evaluated the spectroscopic and thermal responses of electrospun polyamide 6 and modified keratin blends and established a correlation between the diameter of the nanofibres and the amount of the protein [39]. While the polymer-protein blends are proving to be good options combining the good properties of both, reliable processing methods are far from developed [1], and the use of additive manufacturing techniques explored here provides another approach [40,41].

2. Materials and methods

2.1. Powder preparation

Oxidatively sulfitolysised keratin powder was produced using a previously published method [42] by adding $CuSO_4$ to a slurry of commercially scoured chopped wool fibres in water containing $NaSO_3$, stirring for 4 h, before acid precipitation to a powder which was freeze dried. Standard commercial SLS polyamide (PA12 grade PA2200) and ultra-high molecular weight polyethylene powders were sourced from EOS and Sigma-Aldrich respectively, (particle size range: 50 to 70 μm diameter). Powder compositions were prepared by blending keratin into the PE and PA powders based on weight percentage combinations: 5%keratin-95%PE; 10%keratin-90%PE; 5%keratin-95%PA; and 10%keratin-90%PA.

Scanning electron microscopy (SEM) was used to assess powders and sintered surfaces. Powders were sprinkled onto an adhesive carbon disk, sputter coated with 10 nm gold and imaged on a JEOL 7000F SEM at 15 kV (5 kV for sintered surfaces) in secondary electron imaging mode. Image J (version 1.51k 2017) was used for the shape analysis of powder particles. Micrographs were binarized (threshold = 50%) and particles defined using the automatic wand tool and those missed or clearly in error were corrected manually. Sufficient care was taken to avoid the overlapping of particles.

2.2. Thermal analysis of powders

DSC tests were conducted by one-time heating and cooling with different heating rates to evaluate the activation energy mainly and other thermal properties. Pure keratin and keratin-polymer blends sealed (10 to 15 mg) in 40 μL aluminium pans were heated to 200 °C in a DSC (Thermal Analyser STA 449 F5 Jupiter). The melting temperature range T_m, the enthalpy or latent heat of melting, the recrystallization temperature range T_c, and the enthalpy of fusion for semi-crystalline polymers were determined at a heating rate of 10 °C/min. Several experiments with varied heating and cooling rates (10/7.5/5/2.5 °C/min) were carried out, and the resulting heat flows were measured, to simulate the temperature profiles of the SLS environment (see Supplemental file for elaboration). DSC curves obtained with varying heating rates for each powder combination were used to calculate the activation energy of the crystallization kinetics for each temperature range.

2.3. Analysis of sintered test pieces

Test strips were created from pure powders and blends on a developmental in house selective laser sintering test bed, further details of which were reported elsewhere [43–46]. Single layer strips of 100mm×10mm dimensions were printed with varied laser process parameter conditions. In addition to SEM imaging, the internal organisation of the strips was investigated by thin-section transmission light microscopy of cross sections. Sintered samples, vacuum dehydrated over dry silica gel for a week, were directly embedded in Procure 812 epoxy resin and polymerised at 60 °C for 22 h. 1.5 μm sections cut (Leica UCT ultramicrotome and Diatome histodiamond knife) onto water were placed on glass slides and dried for 1 h at 60–80 °C to help flatten them, before imaging on a transmission light microscope (Leica DM6000B with DFC7000T camera).

Mechanical testing using 3-point bending was based on the ASTM standard procedure. Test specimens were not of standard dimensions, due to practical limitations. Shrinkage and lack of adhesion to the build platform led to slight curling of the specimens and the edges of the samples were trimmed to remove the curling. Tests were carried out using an Instron 4204 with a 10 N load-cell and the load range set to 5% (equivalent full-scale range, 0 to 50 g). Sample width was measured using a precision ruler and the thickness was measured at 3 places using a micrometre and averaged for specimen

thickness calculations. 3-point bending tests used a span width of 24.5 mm and loading and support noses had 4 mm radii. A strain rate of 0.01 mm/min was used to test the samples. The crosshead rates were determined for each sample based on their thickness and ranged from 1.3 to 2.7 mm/min. All samples were conditioned at standard settings of 20 °C and 65% RH for 40 h before flexural testing.

3. Results and discussion

3.1. Powders-particle morphology

The pure keratin powder was of mixed particle size with some smooth particles and some smaller jagged pieces (Fig. 1) while synthetic polymer PE and PA particles were largely potato-shaped. PA is a well-established commercial powder material for SLS processing, with good spreading characteristics on the powder bed [47]. Considerable size variation observed in the PE particles may have affected powder bed flow characteristics. 5% or 10% by weight of keratin was used in the formation of the composites. Keratin amounts beyond this limit were found to result in excessive burning and charring in the polymer composites.

The overall shape and surface irregularities of the single particles determine the sintering nature of the bulk powder bed. SLS powder particles should be as spherical as possible, allowing free flow on the

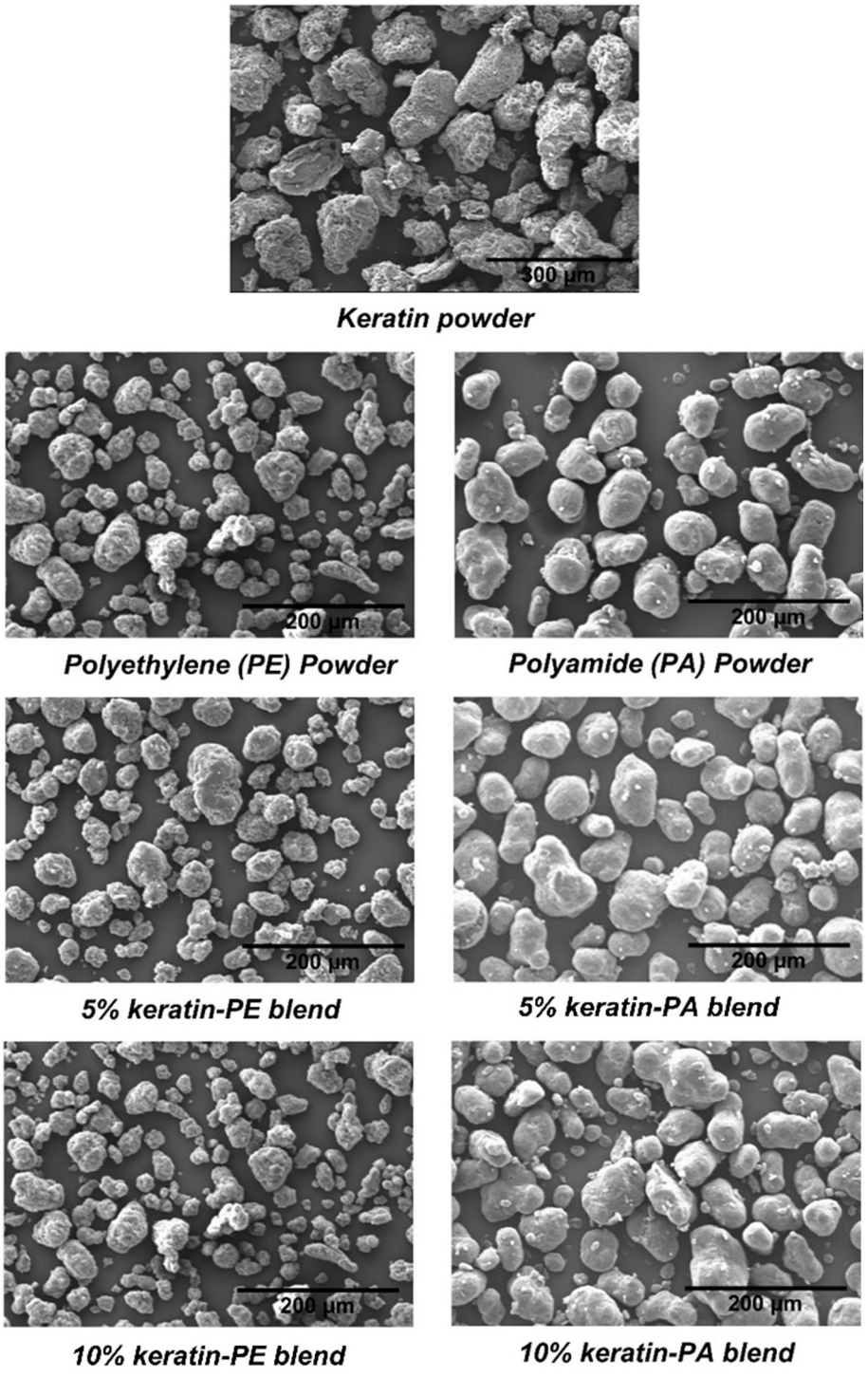


Fig. 1. SEM images of powder particles.

Table 1
Particle size distribution in keratin, PA and PE powders.

Particle diameter (μm)	Frequency		
	Keratin powder	PA powder	PE powder
18–35	21	31	64
35–55	33	35	60
55–80	30	26	10
80–100	17	5	7
100–150	17	2	0

powder bed, and subsequent compaction into substrate layers [48]. The part density is related to the powder bed density which in turn depends on the powder flow and compaction responses. Spherical particles and potato shaped particles are typical of the commercial polymer powders used for selective laser sintering. Freeze dried powder particles often have irregular shapes, adversely affecting the powder flow behaviour and resulting in possible irregular compaction and loss of post consolidation density [49]. The ideal particle size for laser sintering is 20 to 80 μm [50].

The keratin, PA and PE powders used in the current study were analysed for particle sizes and distribution and the results are as listed in Table 1. Images used for the analysis are included in the Supplementary data. Keratin powder particles have the largest range in sample size, from 10 μm to 154 μm, while PA and PE

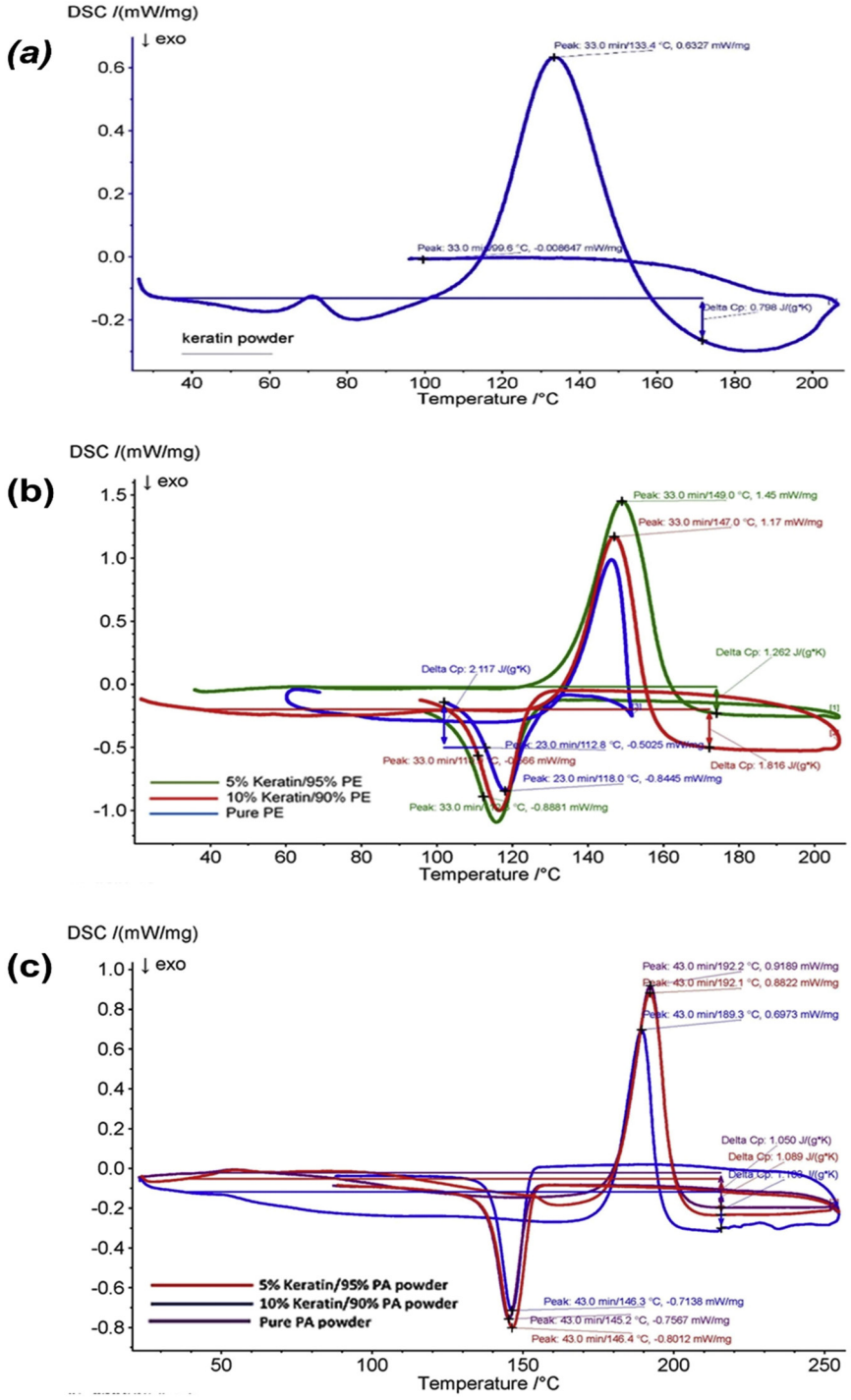


Fig. 2. DSC results (a) keratin (b) keratin-PE blend, and (c) keratin-PA blend powders.

particles varied from 10 μm to 90 μm, with some exceptions in the case of polyamide. The number of larger particles is generally higher in keratin powder compared to PA and PE, which may influence the sintering characteristics. The bulk of the keratin particles were between 30 μm to 80 μm in size, while most PA particles were between30 μm to 70 μm and the PE particles were the smallest at 20 μm to 30 μm. The smaller size range in PE particles is below the optimum size for laser sintering and the effects on the sintering of the smaller particles will be discussed subsequently.

3.2. Differential scanning calorimetry

Differential scanning calorimetry (DSC) can indicate conformational changes in keratin [55] and polymer phase transitions possible by laser sintering [51]. DSC curves generated for the three base materials and the four blends are shown in Fig. 2. Semi-crystalline materials like PA and PE remain hard until the required amount of heat is absorbed and then undergo a rapid change into a viscous liquid, resulting in sharp melting points, as evident in the DSC curves of Fig. 2 [52]. During SLS, with sufficient energy input, the semi-soft polymer flows, forming a solid layer, due to the inter-particle coalescence [53]. As the heated substrate cools below T_m, the polymer crystals nucleate and grow, re-creating regions of ordered molecular chains (crystallites), mingled with the amorphous regions. Above T_m, the polymer will have relatively low viscosity, compared to the amorphous polymers, which favours the rate and amount of consolidation [7].

From the DSC curves in Fig. 2(b) and (c) there were two sharp peaks evident for PE and PA, one during the endothermic melting and the other one during the exothermic crystallization process (crystallization). The temperature range between the crystallization and the melting peaks determines the process window for laser sintering. In the case of pure keratin (Fig. 2(a)), a smaller endothermic peak was noted at 71.1 °C representing the energy required to vaporize the moisture present in the powder [54]. This was followed by a bigger endothermic peak at 133.4 °C likely related to the softening of the keratin due to the plasticisation and loss of bound water as a result of the pressure generated in the closed chamber [55]. During the solidification stages, gradual transitions were observed, without a specific sharp crystallization peak. No protein associated peak was observed in the DSC curves for both keratin-PE and keratin-PA blends, in Fig. 2(b) and (c) respectively, indicating that both PE and PA obscure any keratin-based process. These keratin proteins are complex structures and there is the potential for intra-molecular and inter-molecular interactions to take place. The protein may assume different secondary structures due to the presence of the polymer [54]. Overall, with the addition of keratin, the DSC curves of the PE and PA remained similar, but with subtle changes in the peak levels.

From the DSC curves, the thermodynamic and kinetic parameters, heat capacity (Cp) and glass transition temperature (T_g) were derived as listed in Table 2. The non-isothermal DSC values are measured at different heating rates to generate the Ozawa kinetics plots as shown in Fig. 3, varying the heating rate from 2.5 °C/min to 10 °C/min. The R_2 value of the fit is 0.9373. The heat capacity and the activation energy values obtained from the evaluation of the Ozawa plots are included in Table 2. The results suggest that the plasticised softening temperature of pure keratin powder is 133.4 °C, which is lower than that of the PA and PE powders. This has influenced the melting and crystallization nature of the polymer/keratin composites as evident from the data in Table 2. The melting temperature slightly decreased from pure PA to 5% keratin-PA, and 10% keratin-PA blends, while the crystallization temperature increased. This suggests that the crystalline phase of PA may support the thermal stability of the blend at higher temperatures, while the presence of the protein hinders the crystallization process. Hence, keratin modifies the kinetics of formation of PA crystals during cooling.

Upon blending semi-crystalline polymers with other natural polymers, a decrease in the melting temperature is indicative of the miscibility of the natural polymers in the amorphous phase [56]. In keratin-PA composites, there was a rapid increase in the enthalpy due to higher energy absorption levels, which was also evidenced in the decreased activation energy. Consequently, the temperature change (undercooling) near the crystallization temperature is not as severe as at the beginning and the overall kinetics of crystallization. This influenced the layer formation during SLS, resulting in a tendency to curl when a layer was just formed and a new colder powder layer was applied [49]. With the keratin-PE blends, the enthalpy gradually decreased and the activation energy increased due to the presence of keratin. The gradient for the function describing the phase transformation due to crystallization was the highest in the measured temperature interval. This indicates that the keratin-PE composite required more energy to reach the phase transition level. The thermal stability increased and the temperature difference between melting and crystallization is higher with the addition of keratin (PE 28.3 °C, 5% keratin-PE 33.3 °C and 10% keratin-PE 33.7).

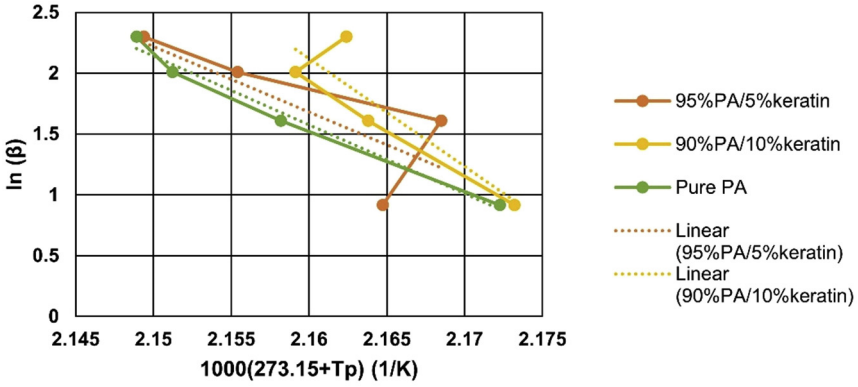
The kinetic and thermodynamic parameters established for the blends from DSC curves were then used to assess the minimum energy density levels required to achieve sufficient melting and inter-particle coalescence (Table 2). Different combinations of the critical process parameters; laser power (P), scan speed (v) and beam diameter (D) can be used to implement the energy density values as needed. Hatch spacing is normally the geometric parameter to control the overlapping of adjacent laser scan tracks. In the current case, the hatch spacing is fixed as equal to the beam diameter. Initial samples were printed to understand the effects of the critical process parameters on the inter-particle bonding and the overall consolidation of the powder materials, by evaluating the layer morphologies. The *a priori* data thus generated was used to establish the mechanical responses of the laser sintered polymer-keratin blends.

3.3. Morphological studies

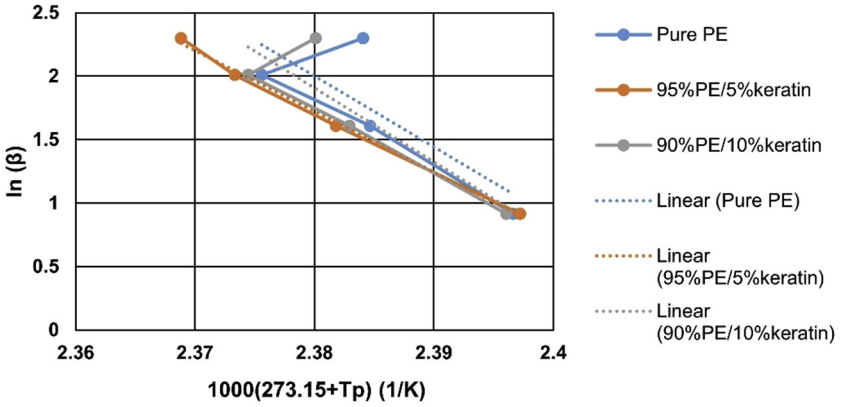
SEM photomicrographs were generated based on single layer samples printed with the range of laser power and scan velocity

Table 2
Kinetic and thermodynamic parameters of PA, PE, keratin/PA and keratin/PE derived from the DSC curves.

Sample	E_a kJ/mol	Glass transition temperature T_g (°C)	C_P heat capacity J/(g°C)	Melting temperature T_m (°C)	Crystallization temperature T_C (°C)	Enthalpy (H) J/g	Minimum energy density predicted from DSC curve J/mm^2	Energy density J/mm^2
Keratin	–	–	0.798	133.4	–	123.3	0.0318	–
PA	699.75	48.3	1.050	192.2	145.2	58.16	0.0386	0.0437
5% keratin-PA	426.08	46.9	1.089	192.1	146.4	83.93	0.0311	0.037
10% keratin-PA	447.01	46.4	1.103	189.3	146.3	90.16	0.0302	0.037
PE	441.68	60.7	2.117	146.3	118	190.4	0.0408	0.044
5% keratin-PE	378.38	67.8	1.262	149	115.7	191.7	0.0473	0.042
10% keratin-PE	459.78	69.9	1.816	150.1	116.4	156.1	0.0431	0.044



(a) Pure PA, 95% PA/5% keratin, and 90% PA/10% keratin powders

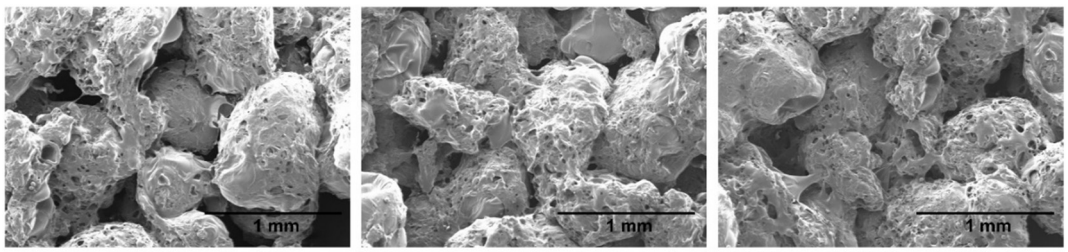


(b) Pure PE, 95% PE/5% keratin and 90% PE/10% keratin powders

Fig. 3. Ozawa plots.

settings selected, with energy density conditions varied around the optimum levels predicted and as listed in Table 2. These images were helpful in evaluating the influences of the laser parameters on the melt-flow behaviour of the powder particles, inter-particle fusion and coalescence. Non-blended keratin powder (energy density range 0.02 J/mm^2 to 0.041 J/mm^2) had a critical energy density identified at 0.03 J/mm^2. Although the keratin powder was not expected to have any thermoplastic properties, we observed distinct structures at each of the settings that connected adjacent particles and which were not present before treatment. These structures resembled melted necks observed in thermoplastic materials, but we were unable to confirm their exact nature. At low energy density (Fig. 4a) the structures were sparsely distributed and narrow. With increased power at the same velocity (Fig. 4b) there was an increase in the density of the interconnecting structures, giving rise to a slight improvement in the overall inter-particle coalescence, but higher energy density combined with a lower scan speed gave no notable increase in structure morphology or density (Fig. 4c). During these tests, keratin powder began charring and decomposing with increased energy density. Unlike PE and PA, the keratin used here is a complex mixture of intermediate filament proteins and fragments of protein. The fact that some formation of necks between keratin particles was observed could be due to a specific keratin protein, or decomposition. While keratin responded to the consolidation by laser exposure, the resulting layers were too fragile for mechanical testing and likely not suitable for practical applications.

Supplementary data (Figs. S4 to S9) may be referred to for a



(a) Power = 6 W, Speed= 500 mm/s
Energy density= 0.02 J/mm²

(b) Power = 9 W, Speed= 500 mm/s
Energy density= 0.03 J/mm²

(c) Power = 9 W, Speed= 400 mm/s
Energy density = 0.041 J/mm²

Fig. 4. Selective laser sintering of keratin.

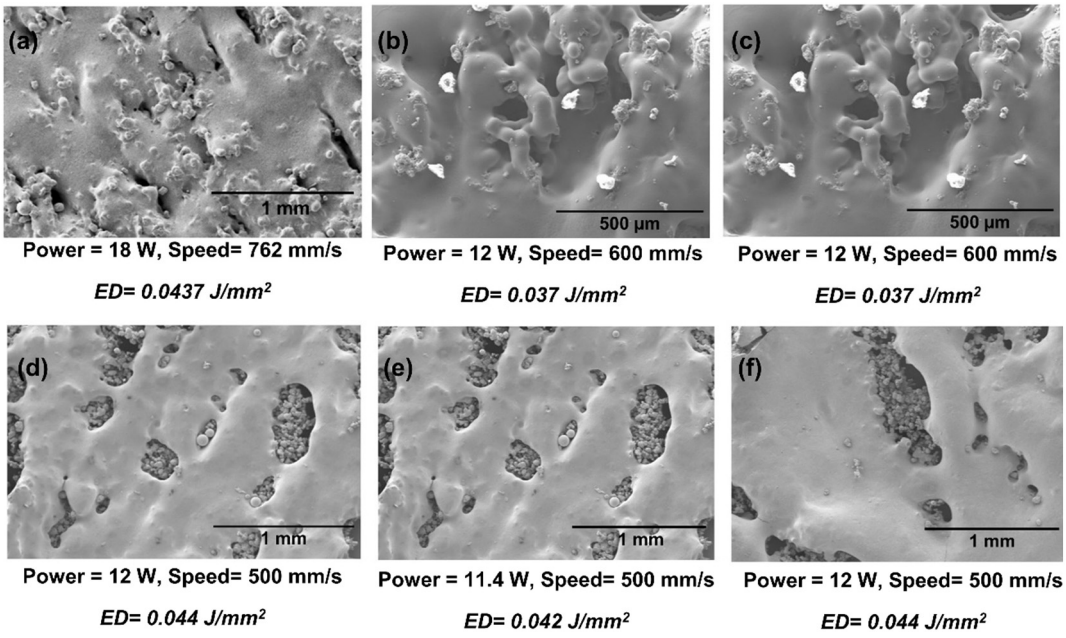


Fig. 5. SEM image of single layer sintered samples with optimum process parameters.

detailed insight into the mechanism of powder consolidation through the SEM images generated based on the printed with base polymers and the keratin polymer blends, with varying laser sintering parameters. Both laser power and scan speed settings influence the inter particle coalescence and in general, the inter-particle and strand coalescence improved with either decreasing the scan speed or increasing the laser power up to certain limits. Blends of PA and 5% and 10% keratin were observed to have improved coalescence and layer formation compared to pure PA at similar powers and speeds. The presence of keratin particles appears to improve the polymer flow and leading to a reduction in the energy required to fuse the keratin-PA blends compared to PA alone, which is also being a prediction from the thermal data. The intra-layer coalescence has also markedly improved in the keratin-PE blends. From a purely particle coalescence point of view, the keratin-PE blends sintered well, but the power levels used to achieve these results also led to protein pyrolysis/charring which may have been the cause for the increased curling of the layers. Based on the results of these initial sintering experiments, the SEM images of the best sintered samples in each case are compiled in Fig. 5, and the corresponding energy density levels are listed in the last column of Table 2.

3.4. Mechanical properties

Single layer rectangular specimens of each material combination were printed using the optimised conditions (Table 2) for mechanical characterisation. Samples containing keratin were noted to have darkened to varying degrees. The keratin-PE blend appeared more sensitive to laser heating and the 10% keratin-PE blend sample was too brittle to be reliably mounted for mechanical testing. The other specimens were subjected to 3-point bending and tensile tests (Figs. S10 to S15). The testing parameters for 3-point bending tests were determined from initial trials using sample 2 (5% keratin-PA blend, 9 W at 600 mm/s). It was noted that the sample did not break within the limits of deflection that could be achieved (at which point the sample started to interfere with the bending rig). Deflection of the samples was stopped once the load had reached a maximum and levelled off (normally close to 90°). Successive tests on sample 2 indicated that the test data was repeatable and the sample recovery between tests was good.

Each sample was then tested first with the brown side up (BSU) and then turned over and tested with the white side up (WSU). Minor differences were noted between the two settings for individual samples, but no consistent pattern emerged, and inter-

Table 3
Results of mechanical tests.

Sample ID	Laser power (W)	Speed (mm/s)	Average thickness (mm)	Width (mm)	Orientation	Modulus of elasticity (MPa)	Peak flexural strength (MPa)	Strain at peak load %	Tensile strength (MPa)
1	9	600	0.588	11.2	–	316.0	7.56	3	9.94
2	9	600	0.719	9.1	BSU	31.4	0.94	4.1	0.176
					WSU	26.7	0.87	4.0	
3	12	600	0.833	6.8	BSU	145.7	4.60	4.7	0.292
					WSU	154.2	5.17	4.7	
4	9	600	0.696	9.3	BSU	40.9	1.09	3.4	0.195
					WSU	41.1	1.23	3.9	
5	12	500	0.843	5.4	BSU	125.4	3.65	4.3	0.391
					WSU	117.1	4.10	5.2	
6	12	500	0.392	8.0	BSU	417.9	1.68	0.7	0.244
					WSU	326.8	1.17	0.6	
7	12	500	0.394	9.8	BSU	160.4	1.13	2.5	0.190
					WSU	126.4	0.98	1.9	

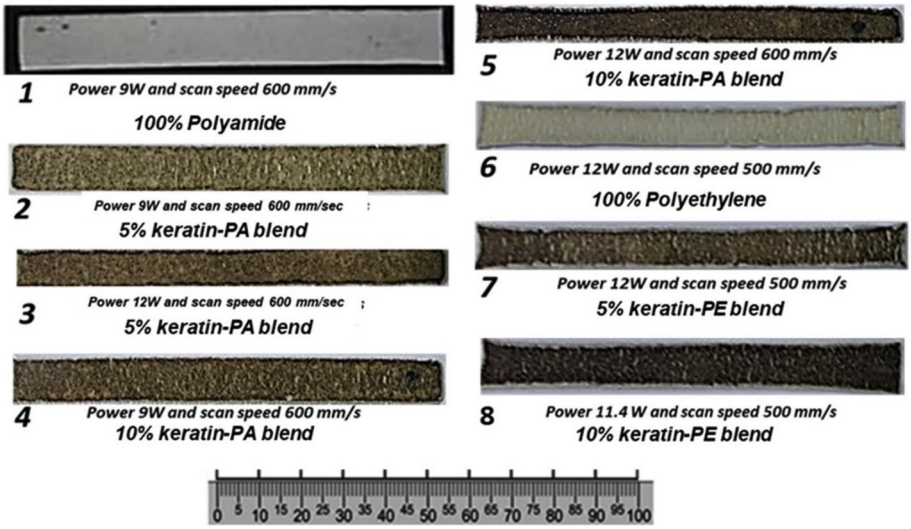


Fig. 6. Single layer printed samples for thin-film mechanical testing.

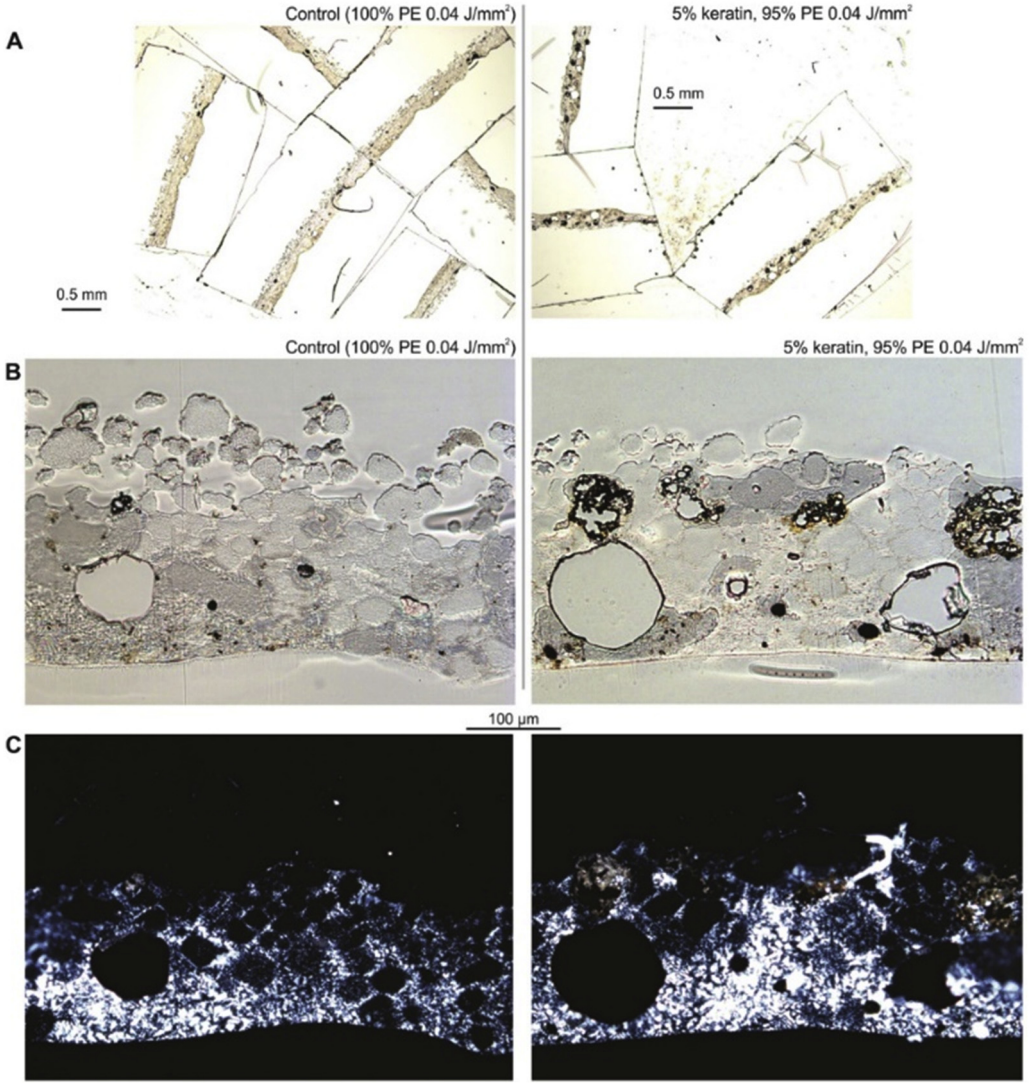


Fig. 7. Cross-sections of sintered samples of PE and keratin-PE blends observed with transmission light microscopy (left, control; right, blend). A. Sections containing sample (stripe). B. Bright-field image of cross sections. C. Polarised light image of cross sections.

sample differences were consistently greater. The flexural strengths of the PA sample were higher than other samples. The mechanical results for the keratin-PA blends followed the general trend that increased power resulted in increased thickness of sample and improved tensile strength. The weakness of the keratin-PA blends may be due to heat-induced changes within keratin particles and subsequent intra-particle void creation possibly through the release of volatiles. Keratin had little impact on the properties of the PE, which was a poor performer mechanically.

3.5. Cross-section structure and keratin-polymer interactions

Transmission light analysis was carried out on the cross-sections of the same samples as used for the mechanical testing (Table 3, Fig. 6). All samples had a clear upper and lower edge; the lower edge was flat (due to the build platform) and the upper edge was granular. In all blends the keratin was patchily distributed and visible as dark inclusions (Fig. 7A). Common features of all samples (including PA and PE samples) were individual polymer particles, voids and small dark inclusions. Inclusion of keratin did not alter the general organisation of the sintered material, but keratin particles appeared as distinct inclusions (Fig. 7B). Crystallinity of the polymer component was not affected noticeably by the inclusion of keratin as observed using polarised light microscopy (Fig. 7C).

In all keratin-containing blends, the keratin particles were clearly yellowed and contained internal voids (Fig. 8A). Some keratin particles were associated with voids in the surrounding polymer (Fig. 8B), but in most cases the interface between the keratin particles and surrounding polymer was continuous and lacked splitting or other signs of separation. It is hypothesised that both yellowing and internal voids within keratin particles may be caused by the heat damage and the consequential release of volatiles (pyrolysis/charring process). Keratin particles appeared similar across the range of laser energy density levels used (Fig. 8). Observations made with keratin-PE (Figs. 7, 8) were similar to those on keratin-PA samples (Fig. S16) and were the same for 5% and 10% keratin inclusion.

4. Conclusion

Keratin and polymer-keratin composites were evaluated for processing by selective laser sintering with varying process conditions. Thermal characterisation has allowed establishment of the working laser energy densities and the evaluation of the morphologies of sintered samples led to the identification of the most suitable energy density levels for each material composition considered. Laser sintering of pure keratin gave interesting results, with some unexpected evidence of coalescence of keratin particles. The reason for the coalescence was not established but is postulated to be as a result of the complex mixture of keratins present in the materials. Mechanical characterisation of samples sintered with the best laser energy densities showed that the presence of keratin significantly slackens the inter-particle bonding achieved through sintering in the case of the keratin-PA combination, while there is a marginal loss with the keratin-PE composite. However, the objective here is to find a means of processing sensitive keratin with the relatively aggressive laser sintering, which has been achieved successfully, based on the current results. Much of this weakness may be due to heat-induced changes within keratin particles and subsequent intra-particle void creation possibly through the release of volatiles. In contrast to this, the polymer and the keratin phase interface appeared to be good when the SEM data is considered. Minimum levels of energy required by polymers for good sintering may still be too high to reduce the keratin damage. Future approaches may find value in focusing on ways of protecting the keratin from heat damage during their brief exposure to the relatively high levels of heat during the sintering process which requires further optimisation of the material and process conditions.

CRediT authorship contribution statement

Sarat Singamneni: Conceptualisation, Formal analysis, Funding acquisition, Methodology, Writing - original draft, Writing - review & editing. **Rajkumar Velu:** Formal analysis, Investigation, Writing - original draft. **Malaya Prasad Behera:** Data curation, Formal analysis, Visualisation. **Sonya Scott:** Conceptualisation, Funding acquisition, Formal analysis, Writing - original draft, Writing - review & editing.

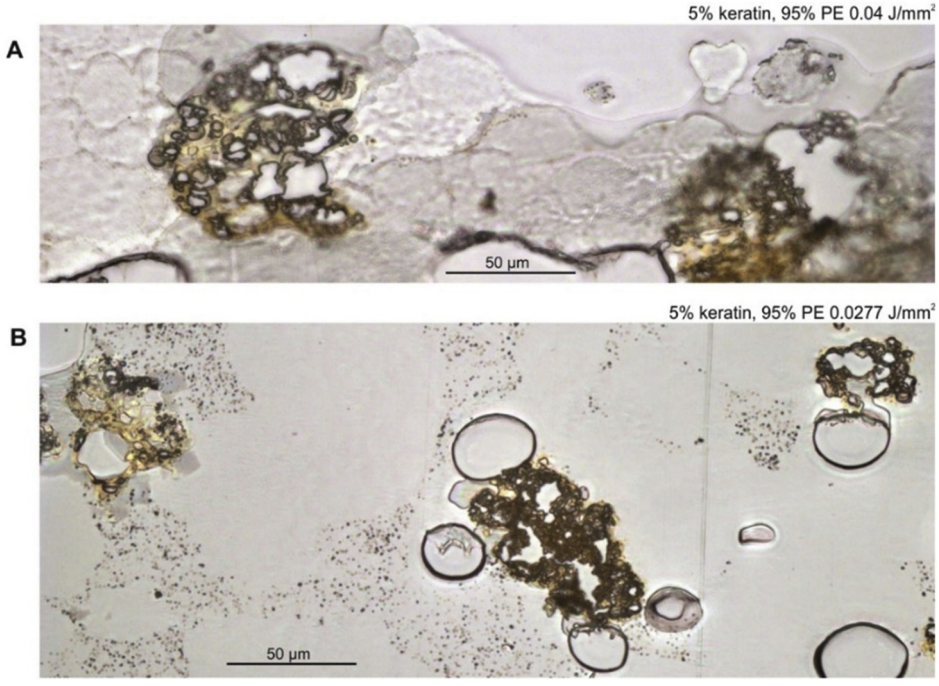


Fig. 8. High magnification of keratin particles within cross-sections of sintered samples created at different levels of energy exposure. 5% keratin and 95% PE at (A) 0.04 J/mm^2 and (B) 0.0277 J/mm^2.

Peter Brorens: Formal analysis, Investigation, Writing - review & editing. **Duane Harland:** Formal analysis, Investigation, Writing - original draft, Visualisation, Writing - review & editing. **Juliet Gerrard:** Conceptualisation, Funding acquisition, Writing - original draft, Writing - review & editing.

Acknowledgement

This research is supported by the National Science Challenge Science for Technological Innovation (SfTI) grant by the Ministry of Business, Innovation and Employment (MBIE) of the New Zealand government.

Appendix A. Supplementary data

Supplementary data to this article can be found online at https://doi.org/10.1016/j.matdes.2019.108087.

References

[1] I. Gibson, D. Rosen, B. Stucker, Additive Manufacturing Technologies: 3D Printing, Rapid Prototyping, and Direct Digital Manufacturing, second edition, 2015.
[2] I. Engelberg, J. Kohn, Physico-mechanical properties of degradable polymers used in medical applications: a comparative study, Biomaterials 12 (3) (1991) 292–304.
[3] R.Q. Frazer, R.T. Byron, P.B. Osborne, K.P. West, PMMA: an essential material in medicine and dentistry, J. Long-Term Eff. Med. Implants 15 (6) (2005) 629–639.
[4] Y. Ikada, Surface modification of polymers for medical applications, Biomaterials 15 (10) (1994) 725–736.
[5] O. Pillai, R. Panchagnula, Polymers in drug delivery, Curr. Opin. Chem. Biol. 5 (4) (2001) 447–451.
[6] D.F. Williams, A. McNamara, R.M. Turner, Potential of polyetheretherketone (PEEK) and carbon-fibre-reinforced PEEK in medical applications, J. Mater. Sci. Lett. 6 (2) (1987) 188–190.
[7] T.H.C. Childs, M. Berzins, G.R. Ryder, A. Tontowi, Selective laser sintering of an amorphous polymer - simulations and experiments, Proc. Inst. Mech. Eng. B J. Eng. Manuf. 213 (4) (1999) 333–349.
[8] G. Bugeda, M. Cervera, G. Lombera, Numerical prediction of temperature and density distributions in selective laser sintering processes, Rapid Prototyp. J. 5 (1) (1999) 21–26.
[9] S. Abashzadeh, M.H. Hajimiri, F. Atyabi, M. Amini, R. Dinarvand, Novel physical hydrogels composed of opened-ring poly(vinyl pyrrolidone) and chitosan derivatives: preparation and characterization, J. Appl. Polym. Sci. 121 (5) (2011) 2761–2771.
[10] S.V. Madihally, H.W.T. Matthew, Porous chitosan scaffolds for tissue engineering, Biomaterials 20 (12) (1999) 1133–1142.
[11] E. Marsano, S. Vicini, J. Skopińska, M. Wisniewski, A. Sionkowska, Chitosan and poly(vinyl pyrrolidone): compatibility and miscibility of blends, Macromol. Symp. 218 (2004) 251–260.
[12] J.M. Wozney, H.J. Seeherman, Protein-based tissue engineering in bone and cartilage repair, Curr. Opin. Biotechnol. 15 (5) (2004) 392–398.
[13] I. Gill, A. Ballesteros, Bioencapsulation within synthetic polymers (part 2): non-sol-gel protein-polymer biocomposites, Trends Biotechnol. 18 (11) (2000) 469–479.
[14] J.U. Otaigbe, D.O. Adams, Bioabsorbable soy protein plastic composites: effect of polyphosphate fillers on water absorption and mechanical properties, Journal of Environmental Polymer Degradation 5 (4) (1997) 199–208.
[15] A.K. Mohanty, M. Misra, L.T. Drzal, Natural Fibers, Biopolymers, and Biocomposites, 2005.
[16] D.P. Harland, J.E. Plowman, Development of hair fibres, in: J.E. Plowman, D.P. Harland, S. Deb Choudhury (Eds.), The Hair Fibre: Proteins, Structure and Development, Springer, New York, 2018, pp. 109–154.
[17] J. McKittrick, P.Y. Chen, S.G. Bodde, W. Yang, E.E. Novitskaya, M.A. Meyers, The structure, functions, and mechanical properties of keratin, JOM 64 (4) (2012) 449–468.
[18] J. Zhang, Y. Li, J. Li, Z. Zhao, X. Liu, Z. Li, Y. Han, J. Hu, A. Chen, Isolation and characterization of biofunctional keratin particles extracted from wool wastes, Powder Technol. 246 (2013) 356–362.
[19] P. Hill, H. Brantley, M. Van Dyke, Some properties of keratin biomaterials: Kerateines, Biomaterials 31 (4) (2010) 585–593.
[20] M. Zoccola, A. Aluigi, A. Patrucco, C. Tonin, Extraction, Processing and Applications of Wool Keratin, Keratin: Structure, Properties and Applications, 2012, pp. 37–62.
[21] V. Verma, P. Verma, P. Ray, A.R. Ray, Preparation of scaffolds from human hair proteins for tissue-engineering applications, Biomed. Mater. 3 (2) (2008).
[22] R. Karthikeyan, S. Balaji, P.K. Sehgal, Industrial applications of keratins - a review, J. Sci. Ind. Res. 66 (9) (2007) 710–715.
[23] A. Aluigi, A. Varesano, A. Montarsolo, C. Vineis, F. Ferrero, G. Mazzuchetti, C. Tonin, Electrospinning of keratin/poly(ethylene oxide) blend nanofibers, J. Appl. Polym. Sci. 104 (2) (2007) 863–870.
[24] S. Murdan, Drug delivery to the nail following topical application, Int. J. Pharm. 236 (1–2) (2002) 1–26.
[25] S. Saravanan, D.K. Sameera, A. Moorthi, N. Selvamurugan, Chitosan scaffolds containing chicken feather keratin nanoparticles for bone tissue engineering, Int. J. Biol. Macromol. 62 (2013) 481–486.
[26] L. Cui, J. Gong, X. Fan, P. Wang, Q. Wang, Y. Qiu, Transglutaminase-modified wool keratin film and its potential application in tissue engineering, Eng. Life Sci. 13 (2) (2013) 149–155.
[27] E. Jin, N. Reddy, Z. Zhu, Y. Yang, Graft polymerization of native chicken feathers for thermoplastic applications, J. Agric. Food Chem. 59 (5) (2011) 1729–1738.
[28] A.A. Onifade, N.A. Al-Sane, A.A. Al-Musallam, S. Al-Zarban, A review: potentials for biotechnological applications of keratin-degrading microorganisms and their enzymes for nutritional improvement of feathers and other keratins as livestock feed resources, Bioresour. Technol. 66 (1) (1998) 1–11.
[29] K. Katoh, M. Shibayama, T. Tanabe, K. Yamauchi, Preparation and physicochemical properties of compression-molded keratin films, Biomaterials 25 (12) (2004) 2265–2272.
[30] K.S. Suslick, M.W. Grinstaff, Protein microencapsulation of nonaqueous liquids, J. Am. Chem. Soc. 112 (21) (1990) 7807–7809.
[31] A. Tachibana, Y. Furuta, H. Takeshima, T. Tanabe, K. Yamauchi, Fabrication of wool keratin sponge scaffolds for long-term cell cultivation, J. Biotechnol. 93 (2) (2002) 165–170.
[32] T. Tanabe, N. Okitsu, K. Yamauchi, Fabrication and characterization of chemically crosslinked keratin films, Mater. Sci. Eng. C 24 (3) (2004) 441–446.
[33] M.N. Taravel, A. Domard, Collagen and its interactions with chitosan: III. Some biological and mechanical properties, Biomaterials 17 (4) (1996) 451–455.
[34] K. Yamauchi, A. Yamauchi, T. Kusunoki, A. Kohda, Y. Konishi, Preparation of stable aqueous solution of keratins, and physiochemical and biodegradational properties of films, J. Biomed. Mater. Res. 31 (4) (1996) 439–444.
[35] R. Deppisch, M. Storr, R. Buck, H. Göhl, Blood material interactions at the surfaces of membranes in medical applications, Sep. Purif. Technol. 14 (1–3) (1998) 241–254.
[36] J.K. Francis Suh, H.W.T. Matthew, Application of chitosan-based polysaccharide biomaterials in cartilage tissue engineering: a review, Biomaterials 21 (24) (2000) 2589–2598.
[37] S.Z. Rogovina, G.A. Vikhoreva, Polysaccharide-based polymer blends: methods of their production, Glycoconj. J. 23 (7–8) (2006) 611–618.
[38] J. Yuan, Z.C. Xing, S.W. Park, J. Geng, I.K. Kang, J. Shen, W. Meng, K.J. Shim, I.S. Han, J.C. Kim, Fabrication of PHBV/keratin composite nanofibrous mats for biomedical applications, Macromol. Res. 17 (11) (2009) 850–855.
[39] M. Zoccola, A. Montarsolo, A. Aluigi, A. Varesano, C. Vineis, C. Tonin, Electrospinning of polyamide 6/modified-keratin blends, E-Polymers 7 (1) (2007) 105.
[40] B. Husar, M. Hatzenbichler, V. Mironov, R. Liska, J. Stampfl, A. Ovsianikov, Photopolymerization-based additive manufacturing for the development of 3D porous scaffolds, Biomaterials for Bone Regeneration: Novel Techniques and Applications 2014, pp. 149–201.
[41] D. Ozdil, H.M. Aydin, Polymers for medical and tissue engineering applications, J. Chem. Technol. Biotechnol. 89 (12) (2014) 1793–1810.
[42] J.A. Maclaren, B. Milligan, Wool Science - The Chemical Reactivity of the Wool Fibre, Science Press, Marrickville, NSW 2204, Australia, 1981.
[43] R. Velu, A. Fernyhough, D.A. Smith, M. Joo Le Guen, S. Singamneni, Selective laser sintering of biocomposite materials, Lasers in Engineering 35 (1–4) (2016) 173–186.
[44] R. Velu, B.P. Kamarajan, M. Ananthasubramanian, T. Ngo, S. Singamneni, Post-process composition and biological responses of laser sintered PMMA and β-TCP composites, J. Mater. Res. 33 (14) (2018) 1987–1998.
[45] R. Velu, S. Singamneni, Selective laser sintering of polymer biocomposites based on polymethyl methacrylate, J. Mater. Res. 29 (17) (2014) 1883–1892.
[46] R. Velu, S. Singamneni, Evaluation of the influences of process parameters while selective laser sintering PMMA powders, Proc. Inst. Mech. Eng. C J. Mech. Eng. Sci. 229 (4) (2015) 603–613.
[47] K. Dotchev, W. Yusoff, Recycling of polyamide 12 based powders in the laser sintering process, Rapid Prototyp. J. 15 (3) (2009) 192–203.
[48] S. Yang, J.R.G. Evans, Metering and dispensing of powder; the quest for new solid freeforming techniques, Powder Technol. 178 (1) (2007) 56–72.
[49] D. Rietzel, B. Wendel, R.W. Feulner, E. Schmachtenberg, New thermoplastic powder for selective laser sintering, Kunststoffe International 98 (2) (2008) 42–45.
[50] N.K. Tolochko, T. Laoui, Y.V. Khlopkov, S.E. Mozzharov, V.I. Titov, M.B. Ignatiev, Absorptance of powder materials suitable for laser sintering, Rapid Prototyp. J. 6 (3) (2000) 155–160.
[51] K. Kaniappan, S. Latha, Certain investigations on the formulation and characterization of polystyrene/poly(methyl methacrylate) blends, Int. J. ChemTech Res. 3 (2) (2011) 708–715.
[52] C.G. Biliaderis, C.M. Page, T.J. Maurice, B.O. Juliano, Thermal characterization of rice starches: a polymeric approach to phase transitions of granular starch, J. Agric. Food Chem. 34 (1) (1986) 6–14.
[53] L. Dong, A. Makradi, S. Ahzi, Y. Remond, Three-dimensional transient finite element analysis of the selective laser sintering process, J. Mater. Process. Technol. 209 (2) (2009) 700–706.
[54] Y. Nakano, Y. Bin, M. Bando, T. Nakashima, T. Okuno, H. Kurosu, M. Matsuo, Structure and mechanical properties of chitosan/poly(vinyl alcohol) blend films, Macromol. Symp. 258 (2007) 63–81.
[55] C. Popescu, The thermodynamics of trichocyte keratins, Adv. Exp. Med. Biol. (2018) 185–203.
[56] M. Liu, Q. Zhao, Y. Wang, C. Zhang, Z. Mo, S. Cao, Melting behaviors, isothermal and non-isothermal crystallization kinetics of nylon 1212, Polymer 44 (8) (2003) 2537–2545.